

## Large-scale shell model calculations for the $N=126$ isotones Po–Pu

E. Caurier,<sup>1</sup> M. Rejmund,<sup>2</sup> and H. Grawe<sup>3</sup><sup>1</sup>*IReS, 23 Rue du Loess, F-67037 Strasbourg, Cedex 2, France*<sup>2</sup>*GANIL, BP 55027, F-14076 Caen, France*<sup>3</sup>*GSI, Planckstrasse 1, D-64291 Darmstadt, Germany*

(Received 4 December 2002; published 21 May 2003)

Large-scale shell model calculations were performed in the full  $Z=82$ – $126$  proton model space  $\pi(0h_{9/2}, 1f_{7/2}, 0i_{13/2}, 2p_{3/2}, 1f_{5/2}, 2p_{1/2})$  employing the code NATHAN. The modified Kuo-Herling interaction was used, no truncation was applied up to protactinium ( $Z=91$ ) and seniority truncation beyond. The results are compared to experimental data including binding energies, level schemes, and electromagnetic transition rates. An overall excellent agreement is obtained for states that can be described in this model space. Limitations of the approach with respect to excitations across the  $Z=82$  and  $N=126$  shells and deficiencies of the interaction are discussed.

DOI: 10.1103/PhysRevC.67.054310

PACS number(s): 21.60.Cs, 23.20.Lv, 27.80.+w

### I. INTRODUCTION

The evolution of proton shell structure beyond  $^{208}\text{Pb}$  is of decisive importance for the shell stabilization of superheavy elements (SHE). To date, the mean field approach is the only viable method to accommodate the large model spaces needed and to predict SHE shell stability [1]. It is known though that mean field predictions of single particle shell structure very often cannot account for the experimental single particle energies (SPE), which are masked by correlations of the  $L=0$  (pairing),  $L=2$  (quadrupole), and/or  $L=3$  (octupole) type [2]. These are often not adequately treated in mean field calculations, though in principal their inclusion is possible. The shell model, on the other hand, using realistic interactions as inferred from free nucleon-nucleon potentials by a perturbative many-body approach [3] yielding the  $G$  matrix as the medium-renormalized potential, includes all types of correlations. Their exploitation, however, is hampered by the stringent truncation schemes needed to handle large model spaces. The development of large-scale shell model codes such as ANTOINE [4] and NATHAN [5–7] has enabled untruncated calculations in the full  $sd$  and  $fp$  major shells, and hence opened the possibility to separate deficiencies of the interactions free from limitations imposed by truncation [8]. For heavier nuclei substantial extensions of the valence space can be handled now.

In the present work we have chosen the  $N=126$  isotones above  $^{208}\text{Pb}$ , where an abundant nuclear data base [9] is available up to  $^{216}\text{Th}$  [10], to perform nearly untruncated shell model calculations for up to 12 protons beyond  $Z=82$ , using a well studied realistic interaction [11,12]. For  $^{216}\text{Th}$  the size of the configuration space for valence protons in the  $Z=82$ – $126$  major shell is comparable to  $^{60}\text{Zn}$  in the  $fp$  shell. Results in previous attempts with various interactions for up to seven protons ( $^{215}\text{Ac}$ ) were severely influenced by the inevitable truncation [13,14]. Excellent agreement was obtained recently for  $^{210}\text{Po}$ ,  $^{211}\text{At}$ , and  $^{212}\text{Rn}$  with a realistic interaction based on the Bonn-A potential [15]. On the other hand, mean field results are available for the  $N=126$  isotones, which with some of the interactions used

seem to indicate a distinct (sub)shell closure at  $Z=92$  [16].

In Sec. II details of the interaction, model space, and code will be described, whereas the results on binding energies, structure of the wave functions, level schemes, and electromagnetic transitions will be discussed in Sec. III. We conclude with a summary of improvements to be applied to the interaction, effective operators, and model space extensions to account for the experimentally observed correlations. Selected results were reported in Refs. [6,17] and for  $^{216}\text{Th}$  in Ref. [10].

### II. INTERACTION, MODEL SPACE, AND CODE

One of the particularly successful approaches to derive an effective realistic residual interaction was that of Kuo and Herling [11,18]. They derived the residual interaction from the free nucleon-nucleon potential of Hamada and Johnston [19] using the reaction matrix techniques developed by Kuo and Brown [20] with renormalization due to the truncated model space. This residual interaction was adopted by Warburton and Brown [12] in the form of

$$\langle j_1 j_2 | V | j_3 j_4 \rangle = \langle j_1 j_2 | V | j_3 j_4 \rangle_{\text{bare}} + K_{ph} \langle j_1 j_2 | V | j_3 j_4 \rangle_{1p-1h},$$

in which the core polarization terms of higher order than  $1p-1h$  are neglected. They found that small modifications to the core polarization component, i.e.,  $K_{ph}=0.90$  result in significantly improved agreement with the experimental spectra. The effective realistic residual interaction as modified by Warburton and Brown [12] has been used in the present calculations. The shell model configuration space included the full  $Z=82$ – $126$  proton major shell beyond  $^{208}\text{Pb}$ , namely, the single proton orbitals  $0h_{9/2}$ ,  $1f_{7/2}$ ,  $0i_{13/2}$ ,  $1f_{5/2}$ ,  $2p_{3/2}$ , and  $2p_{1/2}$ . The single particle energies were taken as determined from the experimental spectrum of  $^{209}\text{Bi}$  [9] with the ground state normalized to  $^{208}\text{Pb}$ , i.e.,  $-3.798$ ,  $-2.902$ ,  $-2.189$ ,  $-0.975$ ,  $-0.679$ , and  $-0.169$  MeV, respectively. The results of these calculations are referred to as SM1. To improve agreement with experiment for high-spin states involving the  $i_{13/2}$  orbital (see Sec. III C 2) a monopole shift of  $+80$  keV was applied to the diagonal two-body ma-

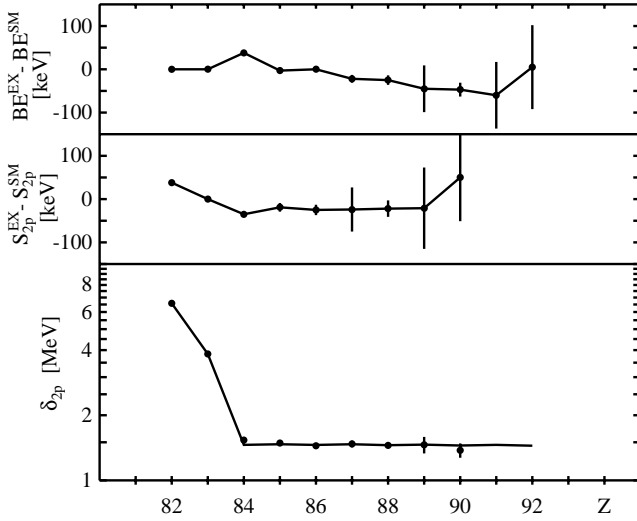


FIG. 1. Shell-model binding energies (upper panel), two-proton separation energies (middle panel), and separation energy differences (lower panel) in comparison to experiment. The upper two panels show deviations in keV, note the log scale in the lower panel.

trix elements (TBME) of the  $h_{9/2}i_{13/2}$  multiplet. As this modification, which will be referred to as model SM2, was found to have only marginal impact on ground state binding energies, wave functions, and transition rates, the SM2 results will be presented for level schemes only.

The calculations are done with the shell model code NATHAN [5–7]. This code works with a coupled basis, diagonalization being done with the standard Lanczos method. For the present study this code is more suited than the  $m$ -scheme code ANTOINE for the following reasons [6].

For semimagic nuclei it is known that the convergence of the wave functions with the seniority is very fast. Taking advantage of the fact that the states of the basis have a defined seniority, the calculation can be done by increasing stepwise the maximal seniority to its full value. This procedure reduces strongly the number of Lanczos iterations.

The basic idea of the two codes is the factorization of the states of the basis in a product of proton and neutron wave functions. To be able to describe semimagic nuclei, the possibility to mix proton and neutron shells in the same subspace or to split the proton (neutron) space in two balanced subspaces was included in the coupled code [6].

A maximum of four broken pairs (seniority 8 for even, 9 for odd mass nuclei) were considered. This enables a full untruncated calculation for all the nuclei up to  $^{217}\text{Pa}$  with matrix dimensions of up to  $1.3 \times 10^6$ .

### III. RESULTS AND DISCUSSION

The results of the shell model calculations are summarized in Figs. 1–8 and Tables I–IV. Basically we will discuss the results obtained with the adopted interaction, single particle energies, and effective operators (model SM1), whereas modifications and improvements (model SM2) will be discussed for level schemes only.

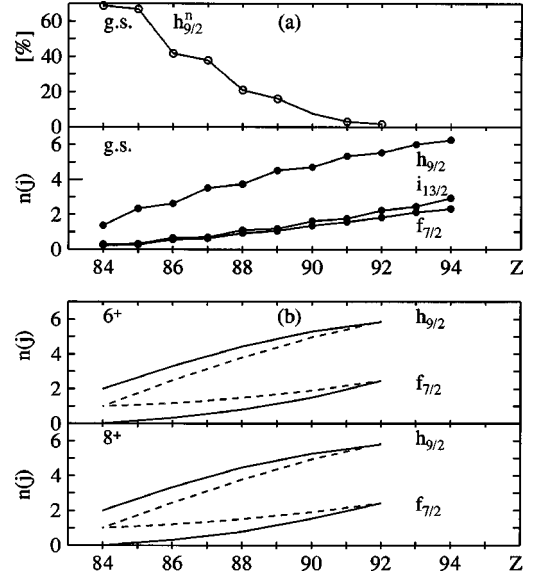


FIG. 2. (a) Percentage of  $0h_{9/2}^n$  configuration,  $n = Z - 82$ , in the g.s. wave functions (upper panel) and occupation numbers in the g.s. of the  $N = 126$  isotones for the high-spin proton orbitals  $0h_{9/2}$ ,  $1f_{7/2}$ , and  $0i_{13/2}$  (lower panel). (b) Occupation of  $0h_{9/2}$  and  $1f_{7/2}$  orbits in the first (full) and second (dashed)  $6^+$  and  $8^+$  states.

#### A. Binding energies

Ground state (g.s.) binding energies (BE) relative to  $^{208}\text{Pb}$  were calculated for the  $N = 126$  isotones  $^{210}\text{Po}$  to  $^{220}\text{Pu}$ . The Kuo-Herling proton-proton ( $pp$ ) TBME include a Coulomb correction averaging  $\sim 250$  keV [11,12]. Following a suggestion by Warburton and Brown [12] an additional shift of  $+49$  keV was applied to all diagonal  $pp$  TBME. Both measures have no influence on excitation energies, but improve g.s. BE [12]. The results are listed in Table I along with experimental values [21] and measured respective predicted spin and parity. The deviations, as shown in the upper panel of Fig. 1, document excellent agreement between shell model and experiment within about 50 keV and imply a high predictive power for g.s. BE beyond the experimentally known nuclei. In the middle and lower panels of Fig. 1 the deviations for the two-proton separation energies  $S_{2p}$ , which show similar quality of agreement, and the separation energy differences  $\delta_{2p}$  are shown. The latter do not exhibit any trace (peak structure) of a subshell closure at  $Z = 92$ , as predicted in some mean field calculations [16].

#### B. Wave functions and configurations

The yrast structure of the  $N = 126$  isotones is determined by the low-lying high-spin orbitals  $\pi 0h_{9/2}$ ,  $1f_{7/2}$ , and  $0i_{13/2}$  (see Table II). In the lower panel of Fig. 2(a) the number of particles in these states, as extracted from the shell model wave functions, is shown. The striking feature is the slow filling of the  $0h_{9/2}$  orbital, which is less than six particles at the foreseen subshell closure  $Z = 92$ . This is nicely corroborated by the percentage of the  $0h_{9/2}^n$  configuration,  $n = Z - 82$ , shown in the upper panel of Fig. 2(a). Note that this configuration at  $Z = 92$  exhausts less than 5% of the wave function. Further inspection reveals that pair scattering is the

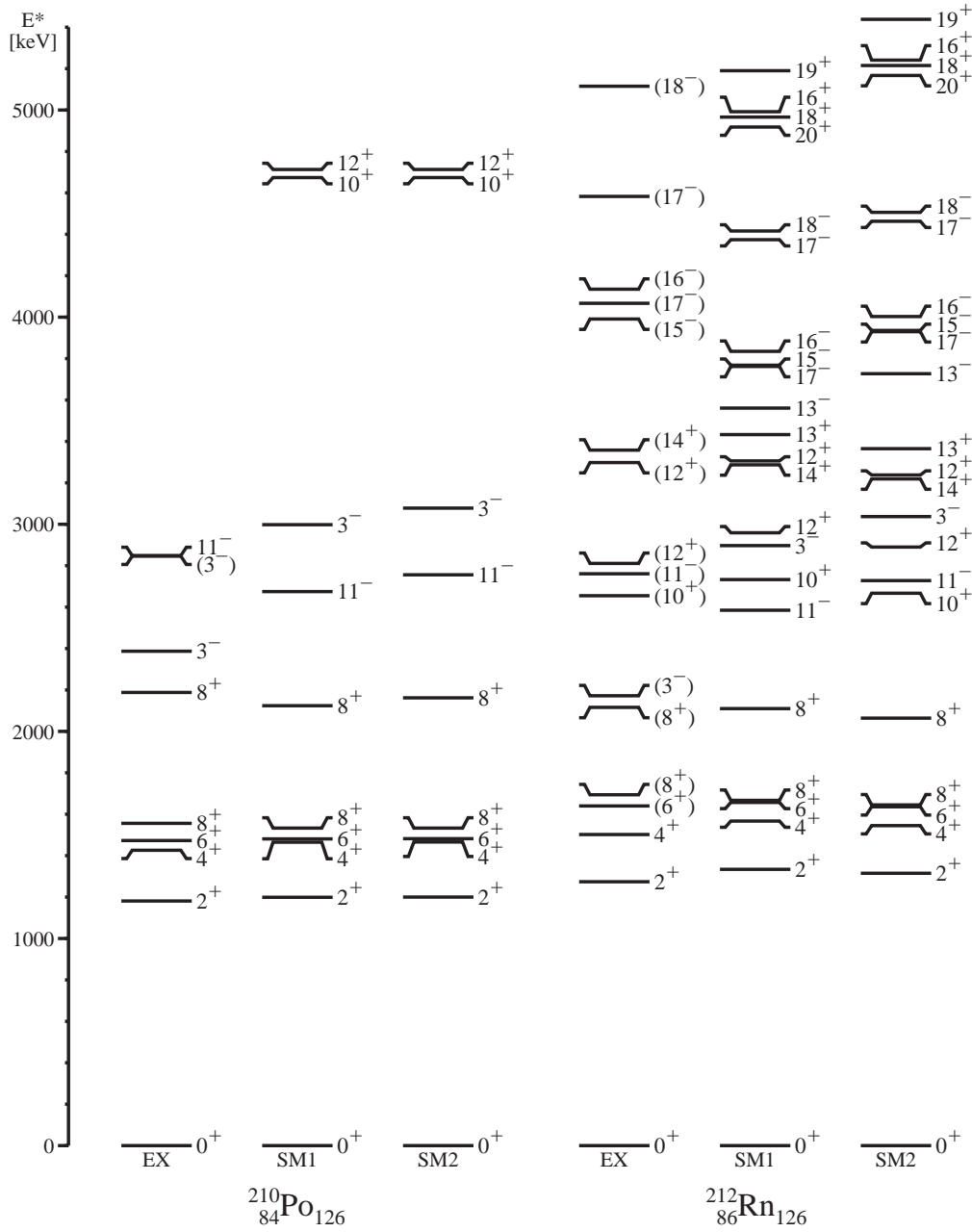


FIG. 3. Shell-model and experimental level schemes for the even  $N=126$  isotones  $^{210}\text{Po}$  and  $^{212}\text{Rn}$  in the model approaches SM1 and SM2. Only near-yrast shell model states are shown and experimental levels have been selected to fit the available model space unless otherwise stated in the text.

underlying mechanism for this result. In Table II for selected  $n$ -quasiparticle (qp) states in  $^{216}\text{Th}$  the leading configurations (partitions) for the high-spin orbitals  $0h_{9/2}$ ,  $1f_{7/2}$ , and  $0i_{13/2}$ , and the percentage of the lowest seniority  $\nu$  are listed. Clearly, with more than 97% all states have unique seniority, proving that pair scattering prevails. The leading partitions demonstrate the  $n$ -qp character of the states, and justify previous attempts to analyze the  $N=126$  isotones in terms of a pairing approach [22].

Further support for the missing  $Z=92$  subshell closure comes from the inspection of the  $I^\pi=6_{1,2}^+$  and  $8_{1,2}^+$  wave functions. The shell occupancies of these states shown in

Fig. 2(b) for the  $h_{9/2}$  and  $f_{7/2}$  orbits feature an almost identical evolution as the g.s. wave functions. The initial difference of  $\pm 1$  for the 2qp states  $h_{9/2}^2$  and  $h_{9/2}f_{7/2}$  is gradually decreasing to zero towards  $Z=92$ , thus indicating continuous filling of the  $f_{7/2}$  orbit by pair scattering. This is confirmed by the fact that the  $6_{1,2}^+$  and  $8_{1,2}^+$  states preserve their 2qp structure with almost pure  $h_{9/2}^2$  and  $h_{9/2}f_{7/2}$  configurations up to  $Z=88$  ( $^{214}\text{Ra}$ ). In  $^{216}\text{Th}$  the  $8_{1,2}^+$  wave functions have about 8% of the minority component and in  $^{218}\text{U}$  the two levels have swapped positions. The  $6_{1,2}^+$  states, on the other hand, are still pure in  $^{216}\text{Th}$  and have a strong 40% admixture of the “minority” component in  $^{218}\text{U}$ . It should be

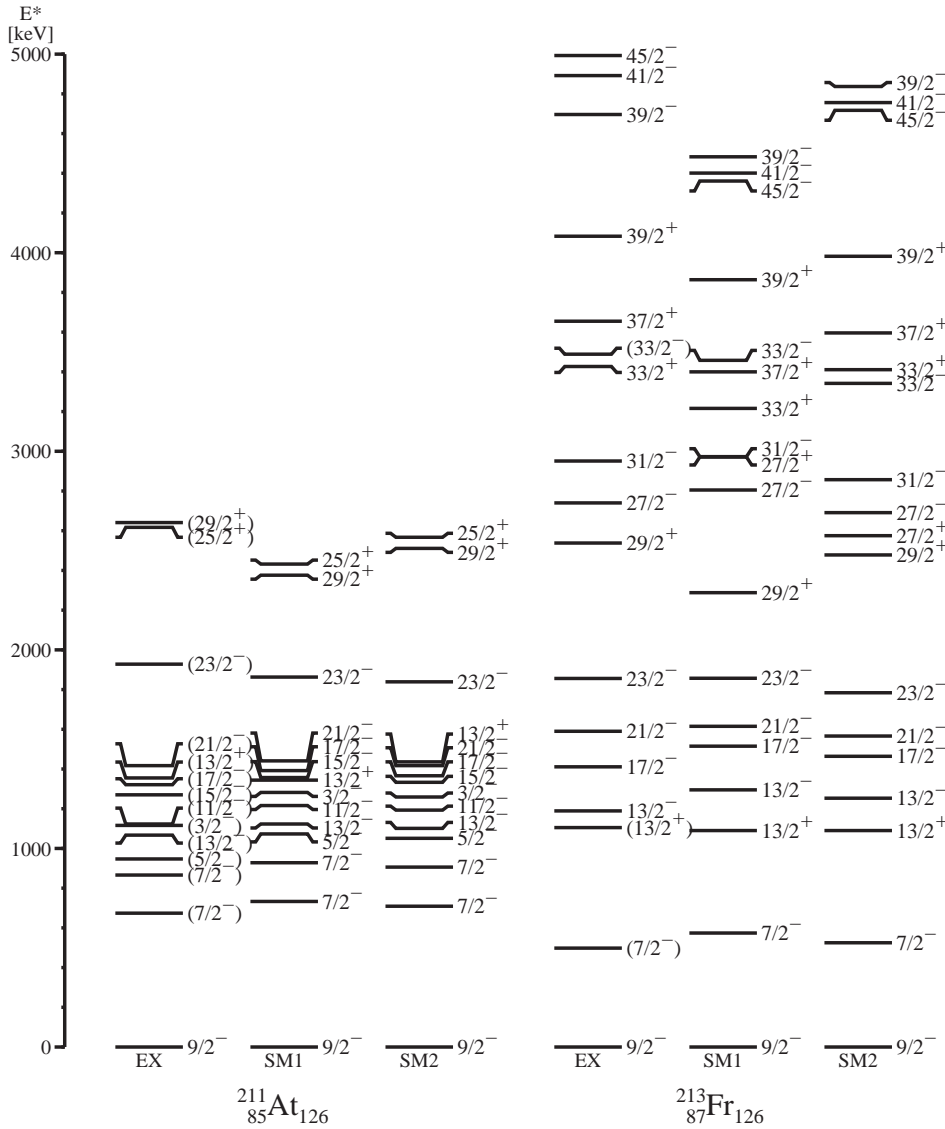


FIG. 4. Same as Fig. 3, but for the odd  $N=126$  isotones  $^{211}\text{At}$  and  $^{213}\text{Fr}$ . See caption of Fig. 3 for further details. For comparison, the low-spin non-yrast states of seniority  $\nu=3$  are shown for  $^{211}\text{At}$ , too.

noted that the  $h_{9/2}$  orbital is filled only to about 60% at  $Z=92$  ( $^{218}\text{U}$ ) in the  $6^+$  and  $8^+$  states, which has implications for the evolution of the  $B(E2)$  between them (see Sec. III D 1). In conclusion, the shell model wave functions clearly reflect the absence of the shell gap as inferred from the binding energies.

**C. Level schemes**

In Figs. 3 and 4 experimental and shell model level schemes are compared for the even and odd  $N=126$  isotones  $^{210}\text{Po}/^{212}\text{Rn}$  and  $^{211}\text{At}/^{213}\text{Fr}$ , respectively, for models SM1 and SM2. Results for  $^{214}\text{Ra}/^{216}\text{Th}$  and  $^{215}\text{Ac}$  are given in Figs. 5 and 6, respectively, for model SM2 along with predictions for  $^{217}\text{Pa}$  (Fig. 6) and  $^{218}\text{U}$  (Fig. 5). Excellent agreement is observed for the low-lying seniority  $\nu=2,3$  states of  $2qp$  and  $3qp$  character up to  $I^\pi=8^+$  and  $21/2^-$ , respectively. This includes the  $23/2^-$  states all the way up to  $^{217}\text{Pa}$ . We notice in passing that also the non-yrast low-spin  $\nu=3$  states in  $^{211}\text{At}$  are well accounted for. In accordance with the miss-

ing subshell closure at  $Z=92$ , the  $I^\pi=8^+$  isomerism is predicted to persist, apart from the  $6^+/8^+$  inversion, which is due to a minor deficiency in the interaction. The steady increase of the  $I^\pi=2^+$  and  $13/2^-$  excitation energies, which is due to the increased pairing in the ground states (see Sec. III B), is also nicely accounted for.

Major deviations can be attributed to two classes of states, which will be discussed in the following.

**1. The  $I^\pi=3^-$  states**

The lowest  $I^\pi=3^-$  states cannot be reproduced for obvious reasons, as the model space does not allow for excitations of the  $^{208}\text{Pb}$  core, especially for neutron  $ph$  excitations. Therefore the yrast  $3^-$  octupole phonon state in  $^{210}\text{Po}$  and the heavier  $N=126$  isotones cannot be accounted for as they are intruders in the present model space. In fact, the lowest  $3^-$  state in  $^{210}\text{Po}$  is calculated close to the experimental  $3_2^-$  level (Fig. 3) belonging to the chosen model space. It should be noticed that the interaction employed in the present work

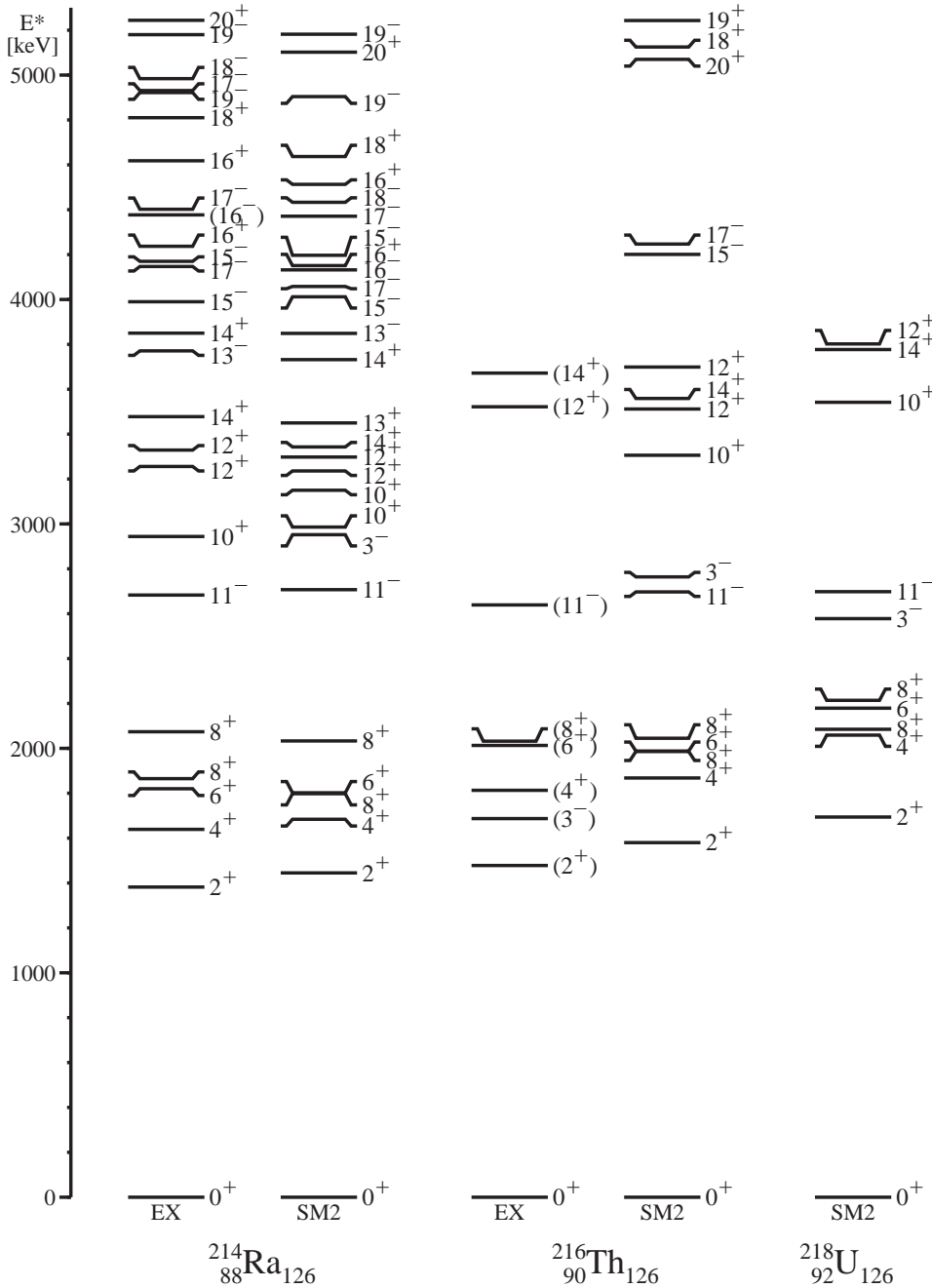


FIG. 5. Shell-model and experimental level schemes for the even  $N=126$  isotones  $^{214}\text{Ra}$ ,  $^{216}\text{Th}$ , and  $^{218}\text{U}$  with a monopole correction of  $+80$  keV applied to the  $0h_{9/2}-0i_{13/2}$  TBME (model SM2).

accounts well for the one- and two-phonon octupole structure in  $^{208}\text{Pb}$  when up to  $2p-2h$  excitations are included [23]. Moreover, the dramatic down-sloping of the  $I^\pi=3^-$  states from 2.615 and 2.387 MeV in  $^{208}\text{Pb}$  and  $^{210}\text{Po}$  to 1.687 MeV in  $^{216}\text{Th}$  [10] is only partly reproduced in the present approach. This has some significance for the predictions of g.s. spins beyond  $^{216}\text{Th}$ , as discussed in Ref. [10]. The coupling of the  $1f_{7/2}$  and  $0i_{13/2}$  orbitals via an  $L=3$  phonon along with the decreasing phonon energy may cause an additional down shift of the  $I^\pi=7/2^-$  state relative to the  $I^\pi=9/2^-$  level, which is predicted to be the g.s. in the shell model calculation (see also Ref. [24]).

### 2. States involving the $0i_{13/2}$ intruder orbital

The odd-parity  $I^\pi=11^- - 19^-$  states in even nuclei and the even-parity  $I^\pi=29/2^+ - 39/2^+$  levels in odd-A nuclei are systematically calculated to be too low in the shell model approach SM1 (Figs. 3 and 4). They have in common active particles in the  $0i_{13/2}$  intruder orbital as likewise the maximum-spin states  $I^\pi=20^+$  and  $45/2^-$  in even and odd nuclei, respectively. As stated in Sec. II, experimental SPE adopted from  $^{209}\text{Bi}$  were used in the calculation. Namely, the  $1f_{7/2}$  and  $0i_{13/2}$  SPE are increasingly distorted by the coupling to the  $L=3$  phonon, as mentioned in the preceding

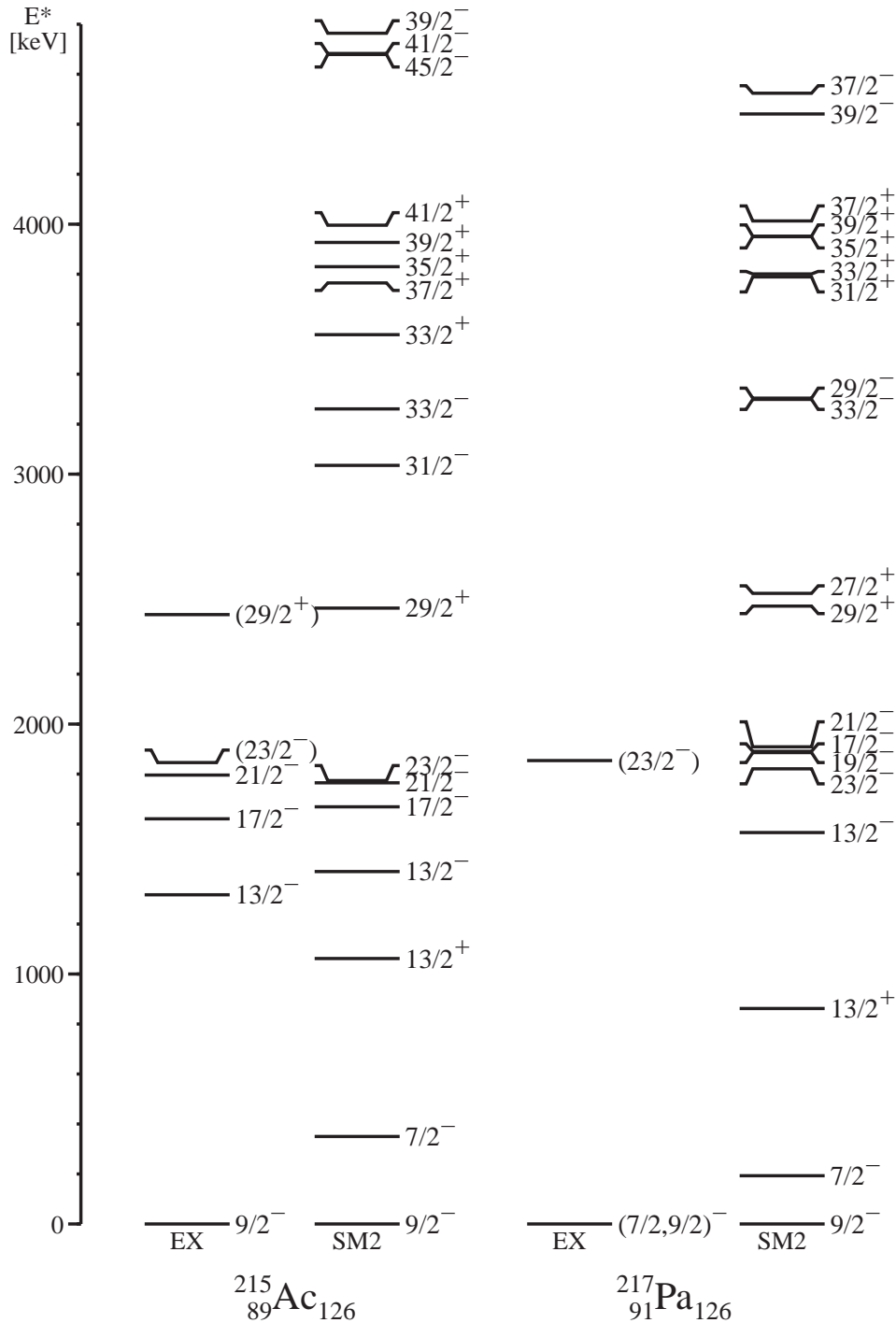


FIG. 6. Same as Fig. 5 for the odd isotones  $^{215}\text{Ac}$  and  $^{217}\text{Pa}$ .

subsection. To account for this, a positive monopole shift of +80 keV was applied to all diagonal  $0h_{9/2} 0i_{13/2}$  TBME. The results are shown for  $^{210}\text{Po}/^{212}\text{Rn}$  and  $^{211}\text{At}/^{213}\text{Fr}$  in Figs. 3 and 4 (SM2). Apart from the few-keV inversion for the maximum-spin state of each quasiparticle configuration the agreement is found to be excellent in model SM2. The quality of agreement persists with increasing number of valence protons for  $^{214}\text{Ra}$ ,  $^{216}\text{Th}$  (Fig. 5), and  $^{215}\text{Ac}$  (Fig. 6). This corroborates the predictive power of the present shell

model approach for isomerism in  $^{218}\text{U}$  (Fig. 5) and  $^{217}\text{Pa}$  (Fig. 6).

It has been suggested earlier that a monopole correction of  $\sim 100$  keV would improve the agreement for levels involving the  $i_{13/2}$  orbital [12]. Two possible origins for this correction have been discussed [12,25]. First, the coupling to the  $L=3$  phonon, which is especially strong for the  $i_{13/2}$  and  $f_{7/2}$  orbitals [10,25], can introduce second order effects that are not accounted for by the effective SPE taken from  $^{209}\text{Bi}$ .

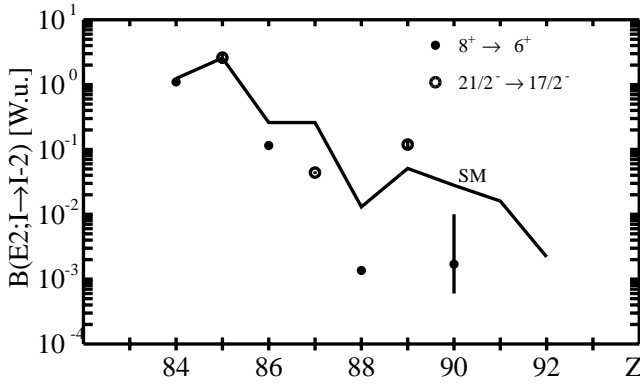


FIG. 7. Shell-model and experimental  $B(E2)$  values for  $\gamma$ -ray transitions from the lowest seniority  $\nu=2,3$  stretched coupled  $I_{max}$  states in even ( $\bullet$ ) and odd ( $\circ$ )  $N=126$  isotones, respectively.

Level shifts may be generated by additional mixing with orbitals that are constituents of the  $L=3$  phonon or by Pauli blocking. The latter may apply for the effective  $i_{13/2}$  state that contains a  $h_{9/2} \otimes 3^-$  component not present in  $f_{7/2}$  [25]. This explains the fact that the suppression in SM1 is largest in the stretched  $h_{9/2}^n i_{13/2}^m$  states as, e.g.,  $I^\pi=11^-, 17^-$  (Fig. 3) and  $I^\pi=29/2^+, 37/2^+, 45/2^-$  (Fig. 4) while levels with  $h_{9/2}^n f_{7/2}$  configurations are not affected.

An alternative scenario for an additional monopole correction is provided by a general deficiency of the Kuo-Herling interaction, as discussed in Refs. [12,26], which may affect the effective TBME between normal and intruder orbits most. The core polarization correction seems to be too large due to an inadequacy in the energy denominators used in the perturbative treatment, while the bare matrix elements are found to be too small due to the use of harmonic oscillator instead of Woods-Saxon radial wave functions.

#### D. Electromagnetic transitions

Further evidence for the pairing and  $L=3$  correlations can be drawn from an analysis of electromagnetic  $E2$  and  $E3$  transition rates, as they depend sensitively on orbit occupation and collective  $E3$  admixtures, respectively. We have refrained from calculating  $M1$  transitions and  $g$  factors for the

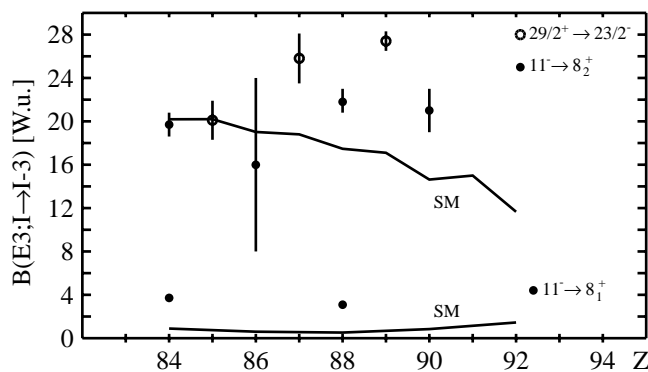


FIG. 8. Shell model predictions and experimental  $B(E3)$  strengths for selected stretched coupled states in even ( $\bullet$ ) and odd ( $\circ$ )  $N=126$  isotones, respectively.

TABLE I. Experimental and shell model binding energies relative to  $^{208}\text{Pb}$ .

Nucleus	$I_{g.s.}^\pi$	Expt. (keV)	SM1 (keV)
$^{210}\text{Po}$	$0^+$	8783(4)	8762
$^{211}\text{At}$	$9/2^-$	11765(5)	11768
$^{212}\text{Rn}$	$0^+$	16065(5)	16065
$^{213}\text{Fr}$	$9/2^-$	18244(9)	18266
$^{214}\text{Ra}$	$0^+$	21885(11)	21910
$^{215}\text{Ac}$	$9/2^-$	23249(50)	23295
$^{216}\text{Th}$	$0^+$	26254(16)	26301
$^{217}\text{Pa}$	$(9/2^-, 7/2^-)^a$	26797(80)	26861
$^{218}\text{U}$	$0^+$	29246(100)	29243
$^{219}\text{Np}$	$a$		28969
$^{220}\text{Pu}$	$0^+$		30739

<sup>a</sup> $9/2^-$  from shell model.

following reason: results obtained in the chosen model space cannot contribute anything to the long discussed question of core polarization contributions to the effective  $M1$  operator [27], as it would allow only to adjust a common  $g_s$  respective  $g_l$  factor. Out of the nine experimentally measured electric quadrupole moments ( $Q$ ) relevant for the present model space, none is known with its sign and only two are model independent measurements [9]. The remaining data rely on calibrations of the electric field gradient in hyperfine experiments using empirical shell model relations between  $B(E2)$  and  $Q$  values assuming pure  $j^n$  configurations (see, e.g., Refs. [28,29]). In the light of the present work, this procedure appears to be highly questionable. Therefore no comparison is made to experimental  $Q$  moment data.

#### 1. E2 transitions

Electromagnetic  $E2$  transition rates were calculated using an effective  $E2$  polarization charge  $\delta_\pi(E2)=0.5e$ . This value, which is routinely adopted for large scale shell model calculations in medium-heavy nuclei as, e.g., in the full  $(p,f)$  model space [8], is larger than  $0.3e$  as estimated from general trends of the isoscalar and isovector giant quadrupole resonance [30]. On the other hand, it is only about half the value inferred for protons and neutrons from the one- and two-particle (hole) neighbors of  $^{208}\text{Pb}$  assuming pure configurations [31,32]. The results for selected  $E2$  transitions in even and odd  $N=126$  isotones are compared to experimental data in Tables III and IV and Fig. 7. The overall agreement is remarkable in view of the fact that the absolute transition strengths vary over about three orders of magnitude in single particle units (W.u.). The agreement for the two- and three-particle nuclei  $^{210}\text{Po}$  and  $^{211}\text{At}$  is noteworthy and corroborates the choice of the polarization charge. The deviation observed for the  $2^+ \rightarrow 0^+$  transition in  $^{210}\text{Po}$  can be ascribed both to a systematic uncertainty in the experimental data as deduced from  $(d,d')$  inelastic scattering [33], and to the neglect of  $^{208}\text{Pb}$   $ph$  excitations in the shell model, which enter most sensitively the  $I^\pi=2^+$  states [34] (see footnote in Table III). We note in passing the simultaneous increase in the shell

TABLE II. Wave functions of selected states in  $^{216}\text{Th}$ . Partitions with more than 10% are listed.

$I^\pi$	$n_{h9}$	$n_{f7}$	$n_{i13}$	$p_{part}$ (%)	$\nu$	$p_\nu$ (%)	qp configuration
$0^+$	6	2	0	20.3	0	99.1	
	4	2	2	17.1			
	6	0	2	13.3			
$2^+$	6	2	0	26.7	2	97.9	$h_{9/2}^2$
	4	2	2	15.9			
	6	0	2	12.3			
$8_1^+$	6	2	0	26.3	2	97.6	$h_{9/2}^2$
	4	2	2	13.5			
	6	0	2	13.1			
$8_2^+$	8	0	0	10.8	2	97.7	$h_{9/2}f_{7/2}$
	5	3	0	22.1			
	7	1	0	22.1			
$11^-$	5	1	2	18.0	2	98.6	$h_{9/2}i_{13/2}$
	5	2	1	27.3			
	7	0	1	19.7			
$14^+$	5	0	3	16.8	4	96.7	$h_{9/2}^3f_{7/2}$
	3	2	3	12.0			
	7	1	0	37.1			
$17^-$	5	3	0	28.3	4	97.7	$h_{9/2}^3i_{13/2}$
	5	1	2	17.3			
	5	2	1	32.7			
$20^+$	7	0	1	30.0	4	98.4	$h_{9/2}^2i_{13/2}^2$
	5	0	3	15.8			
	6	0	2	39.5			
	4	2	2	27.8			
	4	0	4	16.6			

model  $B(E2; 2^+ \rightarrow 0^+)$  and the  $I^\pi = 2^+$  excitation energies from Po to U, which is at variance with generally adopted systematic trends [35]. In Fig. 7, for the maximum-spin states in lowest seniority, the trend with the  $1h_{9/2}$  orbit occupation is analyzed. In a pure and isolated  $h_{9/2}$  shell the  $B(E2; I_{max} \rightarrow I_{max} - 2)$  would develop symmetrically to the middle of the shell, where  $B(E2) = 0$ . This was demonstrated since long for the  $g_{9/2}$  proton and neutron orbitals [36,37]. It is due to the change of sign (from oblate to prolate) for the reduced  $E2$  matrix element for the half-filled shell. It has been stated earlier that the experimental values along the  $N = 126$  isotones up to  $^{215}\text{Ac}$  indicate a shift of the minimum to larger  $Z$  (see Fig. 7) due to scattering of proton pairs into higher-lying orbitals, which slows down the  $h_{9/2}$  filling [22]. Comparing the experimental and shell model trends in Fig. 7, it seems that the shell model approach is even further slowing down the trend, i.e., overemphasizing the pair scattering. The odd-even staggering, both in experiment and shell model, is the remainder of a trivial effect of angular momentum coupling coefficients, which is most prominently seen in the case of an isolated  $j$  shell [37]. Both experiment and shell model break the symmetry with respect to the minimum position. The origin, however, may be twofold. Besides the enhanced pair scattering in the shell model approach, the aforementioned coupling of the  $f_{7/2}$  orbit to the  $L = 3$  phonon and the  $i_{13/2}$  orbit may change the configuration of the yrast  $I^\pi = 8^+$  state in  $^{216}\text{Th}$  [10].

In the shell model approach the latter effect is predicted only for  $^{218}\text{U}$ , as inferred from the wave functions (see Sec. III B). The yrast  $8_1^+$  state has a pure  $h_{9/2}f_{7/2}$  qp structure while the  $6_1^+$  wave function is highly mixed in  $h_{9/2}f_{7/2}$  (40%) and  $h_{9/2}^2$  (60%). The continuous decrease of the  $B(E2)$  values is due to the fragmentation of the wave functions into many components differing in the number of pairs as discussed for the g.s. in Sec. III B, which does not affect their qp structure. This allows, due to particle forbiddance, only diagonal  $E2$  transitions between identical configurations. Furthermore, matrix elements in  $h_{9/2}^n$  configurations with particle ( $n < 5$ ) and hole ( $n > 5$ ) character interfere destructively, while they vanish for  $n = 5$  (midshell) [22,36,37]. Again the trend is determined by pair scattering and the absence of substantial  $h_{9/2}f_{7/2}i_{13/2}$  shell gaps.

## 2. $E3$ transitions

The  $E3$   $\gamma$ -ray transitions beyond  $^{208}\text{Pb}$  are subject to strong distortions by the  $E3$  phonon in  $^{208}\text{Pb}$  [38,39]. Therefore a proper choice of the  $E3$  polarization charge is rather difficult. In a particle-phonon coupling approach to analyze  $E3$  properties of  $^{209}\text{Pb}$  an effective single neutron charge of  $1.3(3)e$  was inferred after correcting for phonon admixtures [24]. Therefore we have chosen somewhat arbitrarily  $\delta_\pi(E3) = 1.4e$  for protons to account for the strong  $E3$  transitions in  $^{210}\text{Po}$  and  $^{211}\text{At}$ . In spite of this normalization, the



TABLE III. Experimental and shell model  $E2$  and  $E3$  strengths for selected transitions in even  $N=126$  isotones in Weisskopf units. Effective polarization charges of  $0.5e$  and  $1.4e$  were used for the  $E2$  and  $E3$  operators, respectively.

$I_i^\pi \rightarrow I_f^\pi$	$^{210}\text{Po}$		$^{212}\text{Rn}$		$^{214}\text{Ra}$		$^{216}\text{Th}$		$^{218}\text{U}$
	EX	SM1	EX	SM1	EX	SM1	EX	SM1	SM1
	$E2$								
$2^+ \rightarrow 0^+$	0.56(12) <sup>a</sup>	3.55		6.41		9.00		11.64	15.18
$4^+ \rightarrow 2^+$	4.53(15)	4.51	1.04(4)	1.51	0.151(4)	0.16		0.039	0.16
$6^+ \rightarrow 4^+$	3.00(12)	3.09	0.40(5)	0.83	0.176(12)	0.050		0.12	0.43
$8_1^+ \rightarrow 6^+$	1.10(5)	1.24	0.115(6)	0.26	0.00136(17)	0.013	0.0017( $^{83}_{11}$ )	0.028 <sup>b</sup>	0.0022 <sup>b</sup>
		0.011		0.014		0.016		0.049 <sup>c</sup>	0.24 <sup>c</sup>
$12_1^+ \rightarrow 10_1^+$		0.89	4.4(2)	3.62		0.062		0.17 <sup>d</sup>	0.71
$12_1^+ \rightarrow 10_2^+$				0.0003		0.038			
$14^+ \rightarrow 12_1^+$			0.032(8)	0.010	0.074(4)	0.006	$\leq 0.25$	0.0001	0.00001
$14^+ \rightarrow 12_2^+$				3.42	0.0149(6)	0.22		0.25	
$15^- \rightarrow 13^-$				4.42	0.56(6)	0.52			
$17^- \rightarrow 15^-$			3.0(16)	2.87	0.025(2)	0.18			
$18^+ \rightarrow 16_1^+$				4.45	0.013(5)	0.0005			
$18^+ \rightarrow 16_2^+$				0.59	2.0(10)	0			
$21^- \rightarrow 19_1^-$				2.39	$\leq 0.5$	0.0002			
$21^- \rightarrow 19_2^-$				0.043	6.5(14)	4.59			
	$E3$								
$11^- \rightarrow 8_1^+$	3.71(10)	0.89	16(8)	0.60	3.09(14)	0.52		0.84	1.45
$11^- \rightarrow 8_2^+$	19.7(11)	20.19		19.02	21.8(10)	17.47	21(2)	14.63	11.66
$17^- \rightarrow 14^+$			16(6)	20.41	25.8(8)	19.00			
$20^+ \rightarrow 17_1^-$			8.6(19)	0.64		0.21			
$20^+ \rightarrow 17_1^-$				29.99		28.43			

<sup>a</sup>Adopted value from  $(d, d')$ ,  $(p, p')$  data yield 1.4(6) W.u. [33].<sup>b</sup>Assuming  $hf$  nature of  $8_1^+$ .<sup>c</sup>Assuming  $h^2$  nature of  $8_1^+$ .<sup>d</sup>Assuming state  $12_2^+$ .

trend with  $Z$  of the shell model and experimental data diverges. This clearly demonstrates that the  $E3$  phonon content in these transitions increases from Po to Th, in agreement with the observation discussed in Sec. III C 1, that the phonon energy decreases from  $\hbar\omega_3 = 2.615$  MeV in  $^{208}\text{Pb}$  to

1.687 MeV in  $^{216}\text{Th}$ . This structure phenomenon is beyond the scope of the present shell model approach. A similar tendency is seen in the remaining  $E3$  transitions between high-spin states listed in Tables III and IV. The observed discrepancies are even worse for weak  $E3$  transitions of

TABLE IV. Experimental and shell model  $E2$  and  $E3$  strengths for selected transitions in odd  $N=126$  isotones in Weisskopf units. Effective polarization charges of  $0.5e$  and  $1.4e$  were used for the  $E2$  and  $E3$  operators, respectively.

$I_i^\pi \rightarrow I_f^\pi$	$^{211}\text{At}$		$^{213}\text{Fr}$		$^{215}\text{Ac}$		$^{217}\text{Pa}$
	EX	SM1	EX	SM1	EX	SM1	SM1
	$E2$						
$17/2^- \rightarrow 13/2^-$		4.47	0.55(4)	0.65	0.08(3)	0.022	0.083
$21/2^- \rightarrow 17/2^-$	2.6(5)	2.57	0.044(2)	0.26	0.12(2)	0.051	0.016 <sup>a</sup>
							0.45 <sup>b</sup>
$29/2^+ \rightarrow 25/2^+$	1.8(5)	1.61		0.35		0.018	0.089
$37/2^+ \rightarrow 33/2^+$			3.7(11)	3.59		0.38	0.37
$45/2^- \rightarrow 41/2^-$			1.8(6)	3.15		0.32	
	$E3$						
$29/2^+ \rightarrow 23/2^-$	20.1(18)	20.2	25.8(23)	18.8	27.4(9)	17.1	15.0
$45/2^- \rightarrow 39/2^+$			46(9)	29.7		27.5	

<sup>a</sup>Assuming  $h^2f$  nature of  $21/2^-$ .<sup>b</sup>Assuming  $h^3$  nature of  $21/2^-$ .

spin-flip type  $i_{13/2} \rightarrow h_{9/2}$  (see Table II for qp configurations), as shown in the lower part of Fig. 8. Obviously, a small admixture of the  $E3$  phonon in the corresponding wave function has more dramatic consequences for a weak transition.

#### IV. CONCLUSION

Shell model calculations for  $N=126$  isotones were performed for the first time in the full proton  $Z=82-126$  model space without truncation up to protactinium ( $Z=91$ ) and with seniority truncation up to plutonium ( $Z=94$ ). The modified Kuo-Herling realistic interaction was found to give an excellent description apart from a small monopole correction that was applied to account for the masking of experimental single particle energies by  $L=3$  correlations. The

main results are summarized as follows: high predictive power for g.s. binding energies up to Pu; no shell gap at  $Z=92$ ; seniority is well preserved; the structure is dominated by pair scattering;  $E3$  correlations are not accounted for.

Further development of the interaction used should comprise an  $L=3$  polarization correction, that can account for position and occupation dependence of the  $I^\pi=3^-$  states. Further experimental evidence can be expected from the study of  $^{217}\text{Pa}$  and  $^{218}\text{U}$ , which seems to be feasible.

#### ACKNOWLEDGMENTS

The authors gratefully acknowledge fruitful discussions with F. Nowacki and A. Byrne.

- 
- [1] M. Bender *et al.*, Phys. Rev. C **60**, 034304 (1999).  
 [2] P.G. Reinhardt *et al.*, RIKEN Rev. **26**, 23 (2000).  
 [3] M. Hjorth-Jensen *et al.*, Phys. Rep. **261**, 125 (1995).  
 [4] E. Caurier, code ANTOINE, Strasbourg, 1989.  
 [5] E. Caurier and F. Nowacki, code NATHAN, Strasbourg, 1997.  
 [6] E. Caurier and G. Martínez-Pinedo, Nucl. Phys. **A704**, 60 (2002).  
 [7] E. Caurier *et al.*, Phys. Rev. C **59**, 2033 (1999).  
 [8] E. Caurier, Phys. Rev. C **50**, 225 (1994).  
 [9] Evaluated nuclear data structure file, <http://www.nndc.bnl.gov/nndc/ensdf/>  
 [10] K. Hauschild *et al.*, Phys. Rev. Lett. **87**, 072501 (2001).  
 [11] T. T. S. Kuo and G. A. Herling, NRL Memorandum Report No. 2258, 1971.  
 [12] E.K. Warburton and B.A. Brown, Phys. Rev. C **43**, 602 (1991).  
 [13] D. Zwarts and P.W.M. Glaudemans, Z. Phys. A **320**, 487 (1985).  
 [14] J.B. McGrory and T.T.S. Kuo, Nucl. Phys. **A247**, 283 (1975).  
 [15] L. Coraggio *et al.*, Phys. Rev. C **60**, 064306 (1999).  
 [16] K. Rutz *et al.*, Nucl. Phys. **A634**, 67 (1998).  
 [17] E. Caurier, in *Proceedings of the 7th International Spring Seminar on Nuclear Physics 2001*, edited by A. Covello (World Scientific, Singapore, 2002).  
 [18] T.T.S. Kuo, Nucl. Phys. **A122**, 325 (1968).  
 [19] T. Hamada and I.D. Johnston, Nucl. Phys. **34**, 382 (1962).  
 [20] T.T.S. Kuo and G.E. Brown, Nucl. Phys. **85**, 40 (1966).  
 [21] G. Audi and A.H. Wapstra, Nucl. Phys. **A624**, 1 (1997).  
 [22] D.J. Decman *et al.*, Z. Phys. A **310**, 55 (1983).  
 [23] B.A. Brown, Phys. Rev. Lett. **85**, 5300 (2000).  
 [24] M. Rejmund *et al.*, Eur. Phys. J. A **8**, 161 (2000).  
 [25] S.J. Poletti *et al.*, Nucl. Phys. **A448**, 189 (1986).  
 [26] I. Bergström *et al.*, Research Institute of Physics, Stockholm, Sweden, Annual Report No. 3.314, 1976.  
 [27] I. Towner *et al.*, Nucl. Phys. **A277**, 285 (1977).  
 [28] E. Mahnke, Hyperfine Interact. **34**, 47 (1987).  
 [29] F. Hardemann, G. Scheveneels, G. Neyens, R. Nouwen, and R. Coussement, Hyperfine Interact. **59**, 13 (1990).  
 [30] I. Hamamoto, in *International Symposium on Nuclear Structure Physics, Göttingen 2001*, edited by R. Casten *et al.* (World Scientific, Singapore, 2001), p. 31.  
 [31] J. Blomqvist, Phys. Scr. **9**, 321 (1974).  
 [32] J.P. Omtvedt *et al.*, Phys. Rev. Lett. **75**, 3090 (1995).  
 [33] C. Ellegaard *et al.*, Nucl. Phys. **A206**, 83 (1973).  
 [34] F. Nowacki, Nucl. Phys. **A704**, 223 (2002).  
 [35] S. Raman, At. Data Nucl. Data Tables **42**, 1 (1989).  
 [36] D.H. Gloeckner *et al.*, Phys. Lett. **40B**, 597 (1972).  
 [37] H. Grawe *et al.*, in *Tours Symposium on Nuclear Physics IV*, edited by M. Arnould, M. Lewitowicz, Yu. Ts. Oganessian, H. Akimune, M. Ohta, H. Utsunomiya, T. Wada, and T. Yamagata, AIP Conf. Proc. No. 561 (AIP, Melville, NY, 2002), p. 287.  
 [38] I. Bergström *et al.*, Phys. Scr. **31**, 333 (1985).  
 [39] G. Dracoulis *et al.*, Nucl. Phys. **A493**, 145 (1989).